Heat and Mass Transport in Microwave Drying of Porous Materials in a Spouted Bed

H. Feng
Dept. of Food Science and Human Nutrition, University of Illinois at Urbana-Champaign, Urbana, IL 61801

J. Tang and R. P. Cavalieri
Dept. of Biological Systems Engineering, Washington State University, Pullman, WA 99164

O. A. Plumb
College of Engineering, University of Wyoming, Laramie, WY 82071

A heat- and mass-transfer model was developed to simulate microwave and spouted-bed combined (MWSB) drying of diced apples, a hygroscopic porous material. A total gas-pressure equation was introduced to take into account internal vapor generation during microwave drying. The governing equations for heat and mass transfer were simplified using a scaling technique and numerically solved with the finite difference method. The physical, thermodynamic, thermal, transport and dielectric properties used in the simulation were either from our measurements or from the literature. Model predictions agreed well with experimental results. The pressure-driven moisture migration during MWSB drying resulted in a high drying rate. The numerical analysis predicted a temperature-leveling effect that was confirmed by experimental results. The unique temperature leveling in MWSB drying helps to control product temperature and improves product quality as compared to microwave-assisted fixed-bed hot-air drying methods.

Introduction

In most industrial drying operations, heat is supplied externally to a product by air or superheated steam to provide energy for moisture evaporation. Heat transfer is therefore in the opposite direction to moisture migration. In addition, as a result of removal of surface moisture during drying, the surface of food materials often shrinks, a phenomenon commonly referred to as case-hardening. Case-hardening significantly increases the resistance to mass transfer at the surface. The dehydrated surface layer also acts as an insulator, resulting in increased resistance to heat transfer. In order to reduce moisture content in foods to a level low enough to prevent undesirable biochemical reactions and microbial growth, prolonged drying time and high temperatures must often be used. This may cause quality degradation in the final products. Freeze-drying, which sublimates moisture under vacuum, can yield high product quality, but production cost is very high. It is therefore desirable to develop new drying techniques that can produce product with relatively low cost and high quality.

Electromagnetic energy at frequencies between 300 MHz and 300 GHz, known as microwaves, directly interacts with moisture and generates heat volumetrically. This eliminates the need to transport heat from the dry surface into the wet core. Microwave energy has been combined with hot-air drying to shorten drying times, especially in the falling-rate periods (Garcia et al., 1988; Prabhanjan et al., 1995; Torringa et al., 1996). Besides increasing the drying rate and improving energy efficiency, microwave drying has the potential to result in better quality, mainly due to a substantial reduction in drying times. Uneven heating, however, has been a major barrier that hinders the commercial application of microwave drying (Mullin, 1995). This barrier has been overcome for particulate materials by combining microwave heating and spouted-bed drying (MWSB) (Feng and Tang, 1998). Experi-

Correspondence concerning this article should be addressed to J. Tang.

ments with heat-sensitive diced apples at moisture content of 22.4% (wet basis) yielded dried products with a uniform and light color. Temperature variations in the products during MWSB drying were within ± 3.5°C. It is desirable to understand the fundamental mechanisms that contribute to the unique performance of MWSB drying for optimized process control and system design.

Microwave drying is accompanied by internal vapor generation as a result of volumetric heating. The internal vapor generation leads to the development of a pressure gradient that helps speed the drying process (Turner and Jolly, 1991). Moisture transport driven by this gas-pressure gradient makes microwave drying distinctly different from conventional hot-air drying. Early works by Le Pourhiet et al. (1982), Jolly and Turner (1989), and Jansen and van der Wekken (1991) used two transport equations to describe the temperature and moisture fields, without considering the pressure effect. Later, Turner and Jolly (1991) considered the contribution of gas pressure to moisture migration and to product quality. They introduced a new transport equation, a total gas-pressure equation, into the drying model. The importance of the additional driving force due to gaseous-pressure gradient in microwave heating has been well recognized in more recent studies of heat and mass transfer conducted by Constant et al. (1996), Torringa et al. (1996), and Ni et al. (1999).

Several physical mechanisms contribute to moisture migration during drying. For a porous solid matrix with free water, bound water, vapor, and air, moisture transport through the matrix can be in the form of either diffusion or capillary flow driven by individual or combined effects of moisture, temperature, and pressure gradients. The predominant mechanisms that control moisture transfer depend on the hygroscopic nature and properties of the materials, as well as the drying conditions, and the way heat is supplied (external/volumetric). In microwave drying, free-water transport has been attributed to diffusion (Torringa et al., 1996; Adu and Otten, 1996) or capillary flow (Wei et al., 1985; Constant et al., 1996; Lian et al., 1997; Turner et al., 1998; Ni et al., 1999). For vapor migration, diffusion (Lian et al., 1997), capillary flow (Turner et al., 1998; Ni et al., 1999), or combination of capillary flow and diffusion (Chen and Schmidt, 1990; Constant et al., 1996) were considered by several research groups as the mechanisms that govern the vapor transport. Few studies considered the migration of bound water, even though it is well known that it behaves differently from free water. There is also no consensus as to the mechanism of bound-water transfer. Turner et al. (1998) assumed that bound-water transfer was caused by diffusion, while Chen and Pei (1989) employed a capillary mechanism to characterize bound-water flow.

Previous efforts in developing comprehensive governing equations for drying have often been hindered by a lack of data for thermal and transport properties. Capillary pressure, intrinsic permeability, relative permeabilities, effective moisture diffusivity, bound-water diffusivity, and thermal conductivity are among the key thermal and transport properties required for a comprehensive simulation of drying. Knowledge of temperature and moisture dependency of these parameters is essential to realistically simulate processes of practical importance. Unfortunately, for hygroscopic porous materials, data for these properties are often not available, especially for foods and agricultural products. For example, few data exist for capillary pressure and bound-water diffusivity of foods and agriculture materials. Permeability data also are not available, except the single-phase permeability data for bread (Goedeken and Tong, 1993). In order to overcome the difficulties, either constant values or data for a different material were used in drying simulations reported in the literature, thus weakening the reliability of the conclusions.

The objectives of this study were (1) to develop a heat- and mass transfer model for MWSB drying of diced apples, a hygroscopic porous material; (2) to simplify the model using scale analysis; and (3) to validate the model with experimental results. An effort was made to consider the moisture and temperature dependency of the thermodynamic, physical, transport, and dielectric properties in the simulation.

Model Development

Assumptions

The assumptions we used in model development are as follows: the material is homogeneous and isotropic on the macroscale; transport of free water is governed by the generalized Darcy's law, which includes the total pressure gradient to account for the effect of microwave volumetric heating; bound-water transport is driven by chemical potential difference (Stanish et al., 1986; Gong, 1992); transport in the gas phase is the result of both convection and diffusion. Other assumptions are as follows.

1. Local thermodynamic equilibrium exists. That is, the solid, liquid, and gas phases are at the same average temperature at any moment in the control volume. This assumption is supported by Turner and Jolly (1991) in a study of dielectric drying of bricks.
2. Solid, liquid, and gas phases are continuous.
3. Binary gas mixture of air and vapor obeys the ideal gas law.
4. Local vapor pressure as a function of moisture content and temperature can be estimated using sorption isotherms.
5. The model material used in this study, diced apples, can be treated as an equivalent sphere.
6. Diced apples are exposed to a uniform microwave field. Although this may not be true at any given moment, over a small time interval the pneumatic agitation of diced apples by the spouted bed moves the pieces so they receive about the same microwave radiation. This assumption is based on the uniform color observed in dried diced apples and the small temperature variations among apple pieces measured during MWSB drying (Feng and Tang, 1998).
7. Electromagnetic field intensity is uniform throughout diced apples. This can be justified by comparing the penetration depth of 2,450 MHz microwave in diced apples to the size of the apple pieces (5 mm in diameter). Penetration depth is a measure of the decay of microwave energy when it is traveling into a material. It is defined as the depth from surface to where the magnitude of the incident microwave decays to 37% (or $1/e$) of its surface value. For 2,450 MHz microwave energy, the penetration depth in the diced apples is 26 mm at 25% moisture content (wet basis), while at 4% moisture content, the penetration depth is 360 mm. Both are significantly larger than the dimension of diced apples used in this study.

The governing equations for microwave drying were derived at a macroscopic level. Variables used in this study are averaged values over a control volume. This approach was first proposed by Whitaker (1977) and has been widely used in heat- and mass-transfer studies related to drying of porous media (Bories, 1991).

Transport relations

Fluid velocities in a multiphase porous medium are given by the generalized Darcy's law:

$$\boldsymbol{u}_f = -\frac{Kk_{rf}}{\mu_f}(\nabla P_f - \rho_f \boldsymbol{g}) = -\frac{Kk_{rf}}{\mu_f}(\nabla P_g - \nabla P_c - \rho_f \boldsymbol{g}) \quad (1)$$

$$\boldsymbol{u}_g = -\frac{Kk_{rg}}{\mu_g}(\nabla P_g - \rho_g \boldsymbol{g}), \quad (2)$$

where the capillary pressure, P_c, is defined as $P_c = P_g - P_f$. The application of Darcy's law requires the fluid to be Newtonian, incompressible, immiscible and with negligible inertial and viscous effects (Bories, 1991). The introduction of relative permeability k_{rf} and k_{rl} takes into account the competition between the liquid and gas flow inside the capillaries and extends Darcy's law to unsaturated porous media.

Diffusive flux of vapor and air is governed by Fick's law:

$$j_v = -j_a = -\rho_g D_{av} \nabla\left(\frac{\rho_v}{\rho_g}\right). \quad (3)$$

Fick's law is valid when the medium's pore size is large compared to the mean molecular free path and when diffusion due to temperature and pressure effects are not important. In apples, the size of intercellular spaces is in the range of 2.6×10^{-4} to 6.7×10^{-4} m, while the size of the parenchyma cells is in the range of 6.7×10^{-5} to 4.9×10^{-4} m (Mohsenin, 1986). The mean free path of vapor at 1 atm is about 2.6×10^{-7} m (Willian, 1998), which is several orders of magnitude smaller than the size of apple cells and intercellular spaces. In drying, the separation of the air–vapor mixture caused by the temperature and pressure gradient is very small and its effect is negligible (Bories, 1991). Hence, Fick's law applies to apples.

In capillary–cellular biomaterials, bound-water migration is very complex. Migration of bound water may take place along very fine capillaries or through the cell wall. Chen and Pei (1989) stated that the bound-water transfer cannot be simply defined as a diffusion process. In the present study, a universal driving force, the chemical potential gradient, was considered as the driving force for the bound-water flow (Gong, 1992). The bound-water flux is written

$$n_b = D_b(1-\epsilon')\frac{\partial \mu_b}{\partial z}. \quad (4)$$

From the local thermodynamic equilibrium, the chemical potential of bound water, μ_b, is equal to the chemical potential of vapor, μ_v. Hence, thermodynamic relations for vapor can be used to express the bound-water flux. Detailed derivation can be found in Stanish et al. (1986), and the resulting equation is given in Eq. 7.

Thermal diffusion is controlled by Fourier's law

$$\boldsymbol{q} = -\lambda_{\text{eff}} \nabla T. \quad (5)$$

In drying problems, the effective thermal conductivity, λ_{eff}, takes into consideration conductive heat transfer through the material as well as heat transfer due to the local evaporation–condensation mechanism (Moyne and Perre, 1991).

Mass fluxes

The liquid, vapor, and air fluxes can be written in accordance with their transport mechanisms as

Free water

$$\boldsymbol{n}_f = \rho_f \boldsymbol{u}_f = -\rho_f \frac{Kk_{rf}}{\mu_f}\nabla P_l = -\rho_f \frac{Kk_{rf}}{\mu_f}\nabla(P_g - P_c). \quad (6)$$

Bound water

$$\boldsymbol{n}_b = \rho_b \boldsymbol{u}_b = -\rho_b D_b(1-\epsilon')\left(\frac{\epsilon}{\rho_v}\nabla P_v - \frac{S_v}{M_v}\nabla T\right). \quad (7)$$

Vapor

$$\boldsymbol{n}_v = \rho_v \boldsymbol{u}_v + \boldsymbol{j}_v = -\rho_v \frac{Kk_{rg}}{\mu_g}\nabla P_g - \rho_g D_{av}\nabla\left(\frac{\rho_v}{\rho_g}\right). \quad (8)$$

Air

$$\boldsymbol{n}_a = \rho_a \boldsymbol{u}_a + \boldsymbol{j}_a = -\rho_a \frac{Kk_{rg}}{\mu_g}\nabla P_g + \rho_g D_{av}\nabla\left(\frac{\rho_v}{\rho_g}\right). \quad (9)$$

Gas

$$\boldsymbol{n}_g = \boldsymbol{n}_a + \boldsymbol{n}_v = -\rho_g \frac{Kk_{rg}}{\mu_g}\nabla P_g. \quad (10)$$

In Eq. 6, the transport caused by gravity is assumed to be negligible; in Eq. 9, $\rho_g = \rho_a + \rho_v$.

Mass balance

The mass-balance equations for free water, bound water, vapor, and air can be written:

Free water

$$(1-\epsilon)\rho_s \frac{\partial X_f}{\partial t} + \nabla\cdot\boldsymbol{n}_f = -\dot{m}. \quad (11)$$

Bound water

$$(1-\epsilon)\rho_s \frac{\partial X_b}{\partial t} + \nabla\cdot\boldsymbol{n}_b = -\dot{m}_b. \quad (12)$$

Vapor

$$(1-\epsilon)\rho_s\frac{\partial X_v}{\partial t}+\nabla\cdot\boldsymbol{n}_v=\dot{m}+\dot{m}_b. \tag{13}$$

Air

$$(1-\epsilon)\rho_s\frac{\partial X_a}{\partial t}+\nabla\cdot\boldsymbol{n}_a=0. \tag{14}$$

Here ρ_s is the density of dry matter.

Heat balance

The total energy balance for a representative elementary volume follows (Bird et al., 1960):

$$\frac{\partial}{\partial t}(\rho h)+\nabla\cdot(\rho\bar{u}h)=-(\nabla\cdot\boldsymbol{q})-(\bar{\tau}:\nabla\boldsymbol{u})+\frac{DP}{Dt}+\Phi \tag{15}$$

(a) (b) (c) (d) (e) (f)

In Eq. 15, (a) is heat storage term; (b) convection term; (c) conduction term; (d) viscous dissipation term; (e) work done by pressure; and (f) internal heat-source term.

The viscous dissipation term $(\bar{\tau}:\nabla\boldsymbol{u})$ and pressure work term (DP/Dt) are usually negligible. Hence, Eq. 15 reduces to an enthalpy balance equation:

$$\frac{\partial}{\partial t}(\rho h)+\nabla\cdot(\rho\boldsymbol{u}h)=-(\nabla\cdot\boldsymbol{q})+\Phi, \tag{16}$$

where

$$\rho h=\rho_s h_s+\rho_v h_v+\rho_a h_a+(\rho_f+\rho_b)h_l \tag{17}$$

$$\rho\boldsymbol{u}h=\rho_v\boldsymbol{u}_v h_v+\rho_a\boldsymbol{u}_a h_a+(\rho_f\boldsymbol{u}_f+\rho_b\boldsymbol{u}_b)h_l. \tag{18}$$

Governing equations

For the spherical geometry considered in this study, mass transfer was assumed to take place only in the radial direction. Hence a one-dimensional problem in spherical coordinates was formulated. The total moisture transport equation can be obtained by adding Eqs. 11–13 and written as

$$\frac{\partial X_l}{\partial t}=\frac{1}{r^2}\frac{\partial}{\partial r}\left[D_X r^2\frac{\partial X_l}{\partial r}+D_T r^2\frac{\partial T}{\partial r}+D_p r^2\frac{\partial P_g}{\partial r}\right], \tag{19}$$

where $X_l\approx X_f+X_b$.

In Eq. 19,

$$\begin{aligned}D_X&=D_X^f+D_X^b+D_X^v\\ D_T&=D_T^f+D_T^b+D_T^v\\ D_P&=D_P^f+D_P^b+D_P^v.\end{aligned} \tag{20}$$

In Eq. 20, moisture transport due to moisture, temperature, and pressure gradients is the sum of the contributions of free water, bound water, and vapor.

The temperature equation was obtained by substituting Eqs. 5, 17, and 18 into the enthalpy balance equation (Eq. 16):

$$C_{TX}\frac{\partial X_l}{\partial t}+C_{TT}\frac{\partial T}{\partial t}=\frac{1}{r^2}\frac{\partial}{\partial r}\left[D_{TX}r^2\frac{\partial X_l}{\partial r}+D_{TT}r^2\frac{\partial T}{\partial r}+D_{TP}r^2\frac{\partial P_g}{\partial r}\right]+\Phi. \tag{21}$$

The total pressure equation was obtained from the air-balance equation (Eq. 14), and can be written as

$$C_{PX}\frac{\partial X_l}{\partial t}+C_{PT}\frac{\partial T}{\partial t}+C_{PP}\frac{\partial P_g}{\partial t}=\frac{1}{r^2}\frac{\partial}{\partial r}\left[D_X^a r^2\frac{\partial X_l}{\partial r}+D_T^a r^2\frac{\partial T}{\partial r}+D_P^a r^2\frac{\partial P_g}{\partial r}\right]. \tag{22}$$

In Eqs. 19, 21, and 22, D_{ij}^k and C_{ij} are kinetic coefficients and capacity coefficients, respectively. The subscripts i and j can be temperature, moisture, or pressure, while the superscript k denotes air, free water, bound water, or vapor. The expressions for these coefficients are given in the Appendix.

Initial and boundary conditions

Initial conditions can be written as

$$\begin{aligned}X_l|_{t=0}&=X_0\\ T|_{t=0}&=T_0\\ P_g|_{t=0}&=P_{\text{atm}}.\end{aligned} \tag{23}$$

Moisture transported to the air–particle interface from the interior of the material leaves the interface as either liquid or vapor, depending upon the intensity of the drying. The moisture flux arriving at the surface from the interior of the material can be expressed as

$$F_{\text{mass}}|_+=(\boldsymbol{n}_f+\boldsymbol{n}_b+\boldsymbol{n}_v)\cdot\boldsymbol{n}=-(1-\epsilon)\rho_s(D_X\nabla X_l+D_T\nabla T+D_P\nabla P_g)\cdot\boldsymbol{n}. \tag{24}$$

Because of the pneumatic agitation in the spouted bed, it is reasonable to assume that once the moisture migrates to the interface, it evaporates immediately and the vapor is carried away by the hot-air stream. The moisture flux leaves the interface by a combination of diffusion and convection and can be expressed as $F_{\text{mass}}|_-=\epsilon h_m(\rho_{vs}-\rho_{v\infty})$. The mass transfer boundary condition in spherical coordinates is then given by

$$-(1-\epsilon)\rho_s\left(D_X\frac{\partial X_l}{\partial r}+D_T\frac{\partial T}{\partial r}+D_P\frac{\partial P_g}{\partial r}\right)\Bigg|_{r=R_0}=\epsilon h_m(\rho_{vs}-\rho_{v\infty}). \tag{25}$$

An energy balance over the interface requires that at the direction normal to the interface, the heat flux arriving at the interface from the interior of the material equals the heat flux leaving the interface by convection, that is, $F_{\text{heat}}|_+ = F_{\text{heat}}|_-$, where

$$F_{\text{heat}}|_+ = \boldsymbol{q}\cdot\boldsymbol{n} + h_a\boldsymbol{n}_a\cdot\boldsymbol{n} + h_v\boldsymbol{n}_v\cdot\boldsymbol{n} + h_l(\boldsymbol{n}_f + \boldsymbol{n}_b)\cdot\boldsymbol{n}$$

$$F_{\text{heat}}|_- = h(T_\infty - T_s) + h_a\boldsymbol{n}_a\cdot\boldsymbol{n} + h_v\boldsymbol{n}_v\cdot\boldsymbol{n} + h_v(\boldsymbol{n}_f + \boldsymbol{n}_b)\cdot\boldsymbol{n}. \tag{26}$$

Thus, the temperature boundary condition is

$$-\lambda_{\text{eff}}\frac{\partial T}{\partial r}\bigg|_{r=R_0} = h(T_\infty - T_s) - \Delta h_v(1-\epsilon)\rho_s \times\left[\left(D_X^l + D_X^b\right)\frac{\partial X_l}{\partial r} + \left(D_T^l + D_T^b\right)\frac{\partial T}{\partial r} + D_P^l\frac{\partial P_g}{\partial r}\right]. \tag{27}$$

The pressure boundary condition can be written as

$$P|_{r=R_0} = P_{\text{atm}}. \tag{28}$$

The symmetry condition at the center of the sphere must be satisfied:

$$\frac{\partial X_l}{\partial r}\bigg|_{r=0} = \frac{\partial T}{\partial r}\bigg|_{r=0} = \frac{\partial P_g}{\partial r}\bigg|_{r=0} = 0. \tag{29}$$

Model Simplification

The equations that govern microwave drying are given in Eqs. 19, 21–23, 25 and 27–29. Liquid moisture content X_l, temperature T, and gas pressure P_g are independent variables. These partial differential equations are coupled and highly nonlinear due to temperature and moisture-dependent coefficients. It is impossible to obtain a closed-form solution to these equations. A numerical approach was therefore used after simplification. To simplify the equations for numerical analysis and to further elucidate the mechanisms, we used a scaling method to analyze the magnitude of each term in the drying equations. The following scaling groups are used (Plumb et al., 1986):

$$r^* = \frac{r}{R_0};\qquad t^* = \frac{t}{t_c};\qquad T^* = \frac{T - T_0}{T_{\max} - T_0};$$

$$P_g^* = \frac{P_g - P_{\text{atm}}}{P_{\max} - P_{\text{atm}}}\qquad X_l^* = \frac{X_l}{X_0};\qquad X_b^* = \frac{X_b - X_e}{X_0 - X_e};$$

$$t_c = \frac{R_0}{u_c} = \frac{\mu_{a\infty}R_0^2}{K_0(P_{\max} - P_{\text{atm}})};\qquad \rho_{vs}^* = \frac{\rho_{vs}}{\rho_{v\infty}} = \frac{P_{vs}}{P_{v\infty}}\frac{T_\infty}{T_s};$$

$$u_c = \frac{K_0}{\mu_{a\infty}}\frac{P_{\max} - P_{\text{atm}}}{R_0}\qquad \Phi^* = \frac{\Phi}{\Phi_0}, \tag{30}$$

where $P_{\max}$ and $T_{\max}$ are the maximum pressure and temperature that might occur in evaporated diced apples during microwave drying; t_c is the time needed for fluid to travel distance R_0 at a velocity due to the maximum pressure gradient in the spherical sample.

Substituting Eq. 30 into Eqs. 19, 21, and 22 we obtained dimensionless drying equations:

$$\frac{\partial X_l^*}{\partial t^*} = \frac{t_c}{R_0^2X_0r^{*2}}\frac{\partial}{\partial r^*}\left[r^{*2}\left(D'_X\frac{\partial X_l^*}{\partial r^*} + D'_T\frac{\partial T^*}{\partial r^*} + D'_P\frac{\partial P_g^*}{\partial r^*}\right)\right] \tag{31}$$

$$C_{TX}\frac{X_0}{t_c}\frac{\partial X_l^*}{\partial t^*} + C_{TT}\frac{T_{\max} - T_0}{t_c}\frac{\partial T^*}{\partial t^*} = \frac{1}{R_0^2r^{*2}}\frac{\partial}{\partial r^*} \times\left[r^{*2}\left(D'_{TX}\frac{\partial X_l^*}{\partial r^*} + D'_{TT}\frac{\partial T^*}{\partial r^*} + D'_{TP}\frac{\partial P_l^*}{\partial r^*}\right)\right] + \Phi_0\Phi^* \tag{32}$$

$$C_{PX}\frac{X_0}{t_c}\frac{\partial X_l^*}{\partial t^*} + C_{PT}\frac{T_{\max} - T_0}{t_c}\frac{\partial T^*}{\partial t^*} + C_{PP}\frac{P_{\max} - P_{\text{atm}}}{t_c}\frac{\partial P_g^*}{\partial t^*} = \frac{1}{R_0^2r^{*2}}\frac{\partial}{\partial r^*}\left[r^{*2}\left(D_X^a\frac{\partial X_l^*}{\partial r^*} + D_T^a\frac{\partial T^*}{\partial r^*} + D_P^a\frac{\partial P_g^*}{\partial r^*}\right)\right]. \tag{33}$$

The expressions for D'_{ij} are listed in the Appendix. The dimensionless boundary conditions are

$$\frac{1}{R_0}\left(D'_X\frac{\partial X_l^*}{\partial r^*} + D'_T\frac{\partial T^*}{\partial r^*} + D'_P\frac{\partial P_g^*}{\partial r^*}\right)\bigg|_{r^*=1} = -\frac{\epsilon\rho_{v\infty}h_m}{(1-\epsilon)\rho_s}(\rho_{vs}^* - 1) \tag{34}$$

$$-\frac{\lambda_{\text{eff}}(T_{\max} - T_0)}{R_0}\frac{\partial T^*}{\partial r^*}\bigg|_{r^*=1} = h(T_\infty - T_0) - hT_s^*(T_{\max} - T_0) - \frac{\Delta h_v(1-\epsilon)\rho_s}{R_0}\left[\left(D_X^l + D_X^b\right)X_0\frac{\partial X_l^*}{\partial r^*} + \left(D_T^l + D_T^b\right) \times(T_{\max} - T_0)\frac{\partial T^*}{\partial r^*} + D_P^l(P_{\max} - P_{\text{atm}})\frac{\partial P_g^*}{\partial r^*}\right] \tag{35}$$

$$P^*|_{r^*=1} = 0 \tag{36}$$

$$\frac{\partial X_l^*}{\partial r^*}\bigg|_{r^*=0} = \frac{\partial T^*}{\partial r^*}\bigg|_{r^*=0} = \frac{\partial P_g^*}{\partial r^*}\bigg|_{r^*=0} = 0. \tag{37}$$

A comparison of the magnitude of each dimensionless group helped to determine which terms were negligible. Since the derivatives in nondimensionless form have order of unity (Willian Deen, 1998), we can determine which term is insignificant by comparing the order of magnitude of the coefficients. In the analysis, a term with coefficient at least one magnitude smaller than the other terms was considered negligible and eliminated from the governing equations. The magnitude for each group was assessed by using literature values of the physical, thermal, and transport parameters in the capacity and kinetic coefficients. For moisture-dependent

parameters, two extreme moistures $X_0 = 7.0$ [dry basis (db)] and $X_1 = 0.1$ (db) were used to estimate the range of the coefficients. For temperature-dependent parameters, an average drying temperature of 343 K was used. In the moisture, temperature, and vapor pressure ranges considered in our analysis, the following transport mechanisms are identified as insignificant through the scaling analysis: (1) in the moisture equation, bound water and vapor flows driven by concentration gradient, free water and vapor flows driven by temperature gradient, and bound water and vapor flows driven by pressure gradient; (2) in the thermal transport equation, the vapor-phase convective-energy transfer caused by moisture gradient; and (3) in the pressure equation, the pressure changes due to rate of changes in temperature and the equivalent pressure gradient due to moisture and temperature gradient. Detailed analyses can be found elsewhere (Feng, 2000), and Eqs. 31–33 are simplified to:

$$\frac{\partial X_l^*}{\partial t^*} = \frac{t_c}{R_0^2 X_0 r^{*2}} \frac{\partial}{\partial r^*}\left[r^{*2}\left(D_{\text{eff}} X_0 \frac{\partial X_l^*}{\partial r^*} + \frac{(P_{\max} - P_{\text{atm}})}{1-\epsilon} \frac{\rho_f}{\rho_s} \frac{Kk_{rf}}{\mu_f} \frac{\partial P_g^*}{\partial r^*} \right) \right] \quad (38)$$

$$(\rho C_p)_{\text{eff}} \frac{T_{\max} - T_0}{t_c} \frac{\partial T^*}{\partial t^*} = \frac{T_{\max} - T_0}{R_0^2 r^{*2}} \frac{\partial}{\partial r^*}\left(\lambda_{\text{eff}} r^{*2} \frac{\partial T^*}{\partial r^*} \right) + \Delta h_v \dot{M} + \Phi_0 \Phi^* \quad (39)$$

$$(1-\epsilon)\frac{\rho_a \rho_s}{\rho_f} \frac{X_0}{t_c} \frac{\partial X_l^*}{\partial t^*} + \frac{\epsilon \zeta M_a}{R'T} \frac{P_{\max} - P_{\text{atm}}}{t_c} \frac{\partial P_g^*}{\partial t^*} = \frac{1}{R_0^2 r^{*2}} \frac{\partial}{\partial r^*}\left[r^{*2} (P_{\max} - P_{\text{atm}}) \rho_a \frac{Kk_{rg}}{\mu_g} \frac{\partial P_g^*}{\partial r^*} \right]. \quad (40)$$

In Eq. 40, ζ is given in the Appendix. The boundary conditions Eqs. 34 and 35 can be simplified to

$$\frac{1}{R_0}\left(D_{\text{eff}} X_0 \frac{\partial X_l^*}{\partial r^*} + \frac{P_{\max} - P_{\text{atm}}}{1-\epsilon} \frac{\rho_f}{\rho_s} \frac{Kk_{rf}}{\mu_f} \frac{\partial P_g^*}{\partial r^*} \right)\Bigg|_{r^*=1} = -\frac{\epsilon \rho_{v\infty} h_m}{(1-\epsilon)\rho_s}(\rho_{vs}^* - 1) \quad (41)$$

$$-\frac{\lambda_{\text{eff}}(T_{\max} - T_0)}{R_0} \frac{\partial T^*}{\partial r^*}\Bigg|_{r^*=1} = h(T_\infty - T_0) - hT_s^*(T_{\max} - T_0) - \frac{\Delta h_v (1-\epsilon)\rho_s}{R_0}\left[D_{\text{eff}} X_0 \frac{\partial X_l^*}{\partial r^*} + \frac{(P_{\max} - P_{\text{atm}})}{1-\epsilon} \frac{\rho_f}{\rho_s} \frac{Kk_{rf}}{\mu_f} \frac{\partial P_g^*}{\partial r^*} \right]. \quad (42)$$

It can be seen from Eqs. 38–42 that terms for capillary pressure were eliminated through the scaling analysis. In Eqs. 36–42, all the thermal and transport properties for apples are either from the literature or measured in separated studies (Feng et al., 2000a,b). The effective moisture diffusivity D_{eff} lumps the contribution of both bound water and free water. From Eq. 38, it can be seen that D_{eff} can be determined with a hot-air only drying test at moderate temperatures in which the internal vapor generation is negligible. Experiments were also designed to measure other important parameters, such as the intrinsic and relative permeabilities, and dielectric properties.

Physical, Thermophysical, and Transport Parameters

Porosity

Porosity of apples as a function of moisture content was obtained using the relation given by Krokida and Maroulis (1999):

$$\epsilon = \frac{1.282 + 1.65(1.89 + X_l)X_l}{(1 + 1.65X_l)(1.899 + X_l)} \quad (43)$$

Vapor pressure

The vapor pressure inside and at the surface of the diced apples is given by its sorption isotherm relation

$$P_v = P_v^0 \varphi(X_l, T). \quad (44)$$

The sorption isotherm $\varphi(X_l, T)$ for apples is given by Feng et al. (1999) by fitting data reported in Roman et al. (1982):

$$X_l = \frac{CX_m a_w}{(1-a_w)[1 + (C-1)a_w]} \left(\text{water activity} \quad a_w = \frac{P_v}{P_v^0}\right), \quad (45)$$

where the parameters X_m and C are given by

$$\ln(X_m) = -7.036 + \frac{1191.2}{T} \quad \text{and} \quad \ln(C) = -9.385 + \frac{3{,}829.1}{T}. \quad (46)$$

Surface heat-transfer and mass-transfer coefficients h and h_m

The Nusselt number in spouted-bed drying is defined as

$$Nu = \frac{hD_c}{\lambda_a}. \quad (47)$$

In spouted-bed drying, Markowski (1992) used a correlation for the Nusselt number:

$$Nu = 0.0045 Ar^{0.226} Re^{0.664}\left(\tan\frac{\gamma}{2}\right)^{-0.852}\left(\frac{H_0}{d_p}\right)^{-1.47} \times \left(\frac{D_c}{d_p}\right)^{0.947} \phi^{2.301}. \quad (48)$$

Table 1. Correlations for Thermal, Thermodynamic, Dielectric, and Mass-Transport Parameters

Parameter	Correlation	Reference
Viscosity of gas, μ_f	$\mu_f(T) = \mu_{f_0} \exp(a - bT + cT^2 + dT^3 - eT^4)$ $\mu_{f_0} = 1\times10^{-4}$; $a = 29.619$; $b = 0.152$; $c = 0.648\times10^{-4}$; $d = 0.815\times10^{-6}$; $e = 0.120\times10^{-8}$	Turner, 1991
Viscosity of free water, μ_g	$\mu_g(T) = \mu_{g_0}\{T^{1/2}/(a + b/T - c/T^2 + d/T^3)\}$ $a = 0.672$; $b = 85.229$; $c = 2111.475$; $d =$ 106417.0; $\mu_{g_0} = 1\times10^{-6}$	Turner, 1991
Latent heat of water, Δh_v	$\Delta h_v = 2.792\times10^6 - 160T - 3.43T^2$	Stanish et al., 1986
Effective thermal conductivity of apple, λ_{eff}	$\lambda_{\text{eff}} = 0.12631 + 0.0595X_l$	Donsì et al., 1996
Thermal conductivity of air, λ_a	$\lambda_a = 0.0035 + 7.67\times10^{-5} * T$	Turner, 1991
Specific heat of apple, $C_{p\text{eff}}$	$C_{p\text{eff}} = 1415 + \dfrac{27.21X_l}{1 + X_l}$	Niesteruk, 1996
Loss factor of apples, ϵ''	$\epsilon'' = a_1 + a_2T + a_3T^2 + a_4X + a_5XT$ $+ a_6XT^2 + a_7X^2 + a_8X^2T + a_9X^3$ $a_1 = -23.5999$; $a_2 = 0.158233$; $a_3 = -0.000256978$; $a_4 = -1.87998$; $a_5 = 0.00768435$; $a_6 = -5.6363\times10^{-6}$; $a_7 = 0.0289568$; $a_8 = -7.66337\times10^{-5}$; $a_9 = -4.09947\times10^{-5}$	Feng et al., 2000b
Effective diffusivity of apple, D_{eff}	$D_{\text{eff}} = a0 * \exp\left(-\dfrac{a1 + a2 * X_l}{T}\right)$ $a_0 = 6.273\times10^{-4}$; $a_1 = 5.843\times10^3$ $a_2 = -2.038\times10^2$	This study

The dimensionless surface mass-transfer coefficient, h_m, is estimated by the Sherwood number:

$$Sh = \frac{h_m d_p}{D_{av}}. \tag{49}$$

The surface mass-transfer coefficient for spouted-bed drying is not available in the literature. The Lewis analogy was used to estimate the Sherwood number, Sh, and hence the mass-transfer coefficient, h_m (Bird et al., 1960). The formulations for particle Archimedes number, Ar, and particle Reynolds number are given in the "Notation" section.

Permeability

The intrinsic permeability $K(\epsilon)$ of apple tissue as a function of porosity has been determined by Feng et al. (2001a). It can be described by a Kozeny-Carman equation:

$$K(\epsilon) = 5.578\times10^{-12}\frac{\epsilon^3}{(1-\epsilon)^2}. \tag{50}$$

Shrinkage during drying can be accounted for in the drying model using the porosity vs. moisture relation given in Eq. 43. The gas and liquid relative permeabilities for apple tissue were also determined (Feng et al., 2001a), and can be correlated to the saturation level S using empirical equations:

$$k_{rg} = 1.01e^{-10.86\,S} \tag{51}$$

$$k_{rl} = S^3. \tag{52}$$

Table 2. Input Parameters Used in Numerical Investigation

Parameter	Unit	Value	Parameter	Unit	Value
X_0		0.2021	ρ_f	$\text{kg}\cdot\text{m}^{-3}$	1,000
T_0	K	295	ρ_s	$\text{kg}\cdot\text{m}^{-3}$	1,650
$P_{\text{atm}} = P_0$	kPa	101.3	ρ_{pb}	$\text{kg}\cdot\text{m}^{-3}$	710
R_0	m	0.0025	$\rho_{v\infty}$	$\text{kg}\cdot\text{m}^{-3}$	1.029
W_s	kg	0.03	D_c	m	0.082
P_{absorb}	W	200	H_0	m	0.09
λ_0	m	0.122	γ	Deg	34.4
T_z	K	343	U	$\text{m}\cdot\text{s}^{-1}$	2.1
$P_{v\infty}$	Pa	9243	$\mu_{a\infty}$	$\text{kg}\cdot\text{m}^{-1}\cdot\text{s}^{-1}$	2.01×10^{-5}
$\rho_{v\infty}$	$\text{kg}\cdot\text{m}^{-3}$	0.0094	K_0	m^2	3.0×10^{-12}
R'	$\text{J}\cdot\text{mol}^{-1}\cdot\text{K}^{-1}$	8.314	N	Node	15
M_v	$\text{kg}\cdot\text{mol}^{-1}$	0.018	TL	s	1,500
M_a	$\text{kg}\cdot\text{mol}^{-1}$	29			

Microwave-power source term Φ

Microwave-power absorption by the sample during drying is given by (Feng, 2000):

$$\Phi = \Phi_0 \frac{\epsilon''}{\epsilon''_0} \tag{53}$$

where Φ_0 is the absorbed microwave power at the beginning of a MWSB drying test. It is given by $\Phi_0 = \Phi_{input} - \Phi_{reflet}$, the difference between measured input and reflected power; and ϵ''_0 is the loss factor corresponding to temperature and moisture content at the beginning of a drying test. Other parameters used in the model are presented in Table 1.

Numerical Analysis

The moisture, temperature, and pressure equations, together with the boundary conditions were solved using the finite difference method. A sphere with a diameter of 5 mm was divided into 15 layers with a thickness $\delta = 1/3$ mm. A time step of 1 s was selected in the simulation. The Crank-Nicolson scheme was used to discretize the partial differential equations for the internal nodes. The boundary conditions at nodes 0 and 16 were discretized with a three-point formula to obtain the same accuracy with internal nodes. The moisture, temperature, and gas-pressure equations were solved simultaneously. Hence, the assembled matrix has a dimension of 48×48. A program was written using MatLab to implement the simulation. The parameters required for the calculation are given in Table 2. Details of the finite difference formulation can be found in Feng (2000).

A numerical test was conducted using different time steps and mesh sizes to examine convergence of the model. With time steps of 2, 1, and 0.5 s, the difference among three time steps in model predictions was less than 0.5% for moisture, temperature, and pressure. The effect of mesh size was examined by dividing the sphere into 10, 15, 30, and 45 elements. The mesh convergence was verified with refined mesh sizes. Time step of 1.0 s and a 15-element mesh size were considered to be appropriate.

Experimental Studies

A combined microwave and spouted-bed dryer was developed for the drying tests to validate the model simulation. This system consisted of a 2.45-GHz microwave supply system and a hot-air system (Figure 1). In the microwave supply system a magnetron generated the microwaves, a waveguide transmitted the waves to the drying cavity, a directional coupler with power meters measured power components. A circulator with a water load was installed to absorb the reflected power. A three-stub tuner was used to adjust the matching impedance into the drying cavity. The power generated from the magnetron could be continuously adjusted using an Akter SM445 power controller. Both the incident and the reflected power were measured using two HP power meters so that the power absorbed by the drying sample was accurately determined.

Diced Red Delicious apples (*Malus domestica Borkh*) with initial moisture content of 20.2% [wet basis (wb)] were used in drying tests. The spouted-bed superficial air velocity was

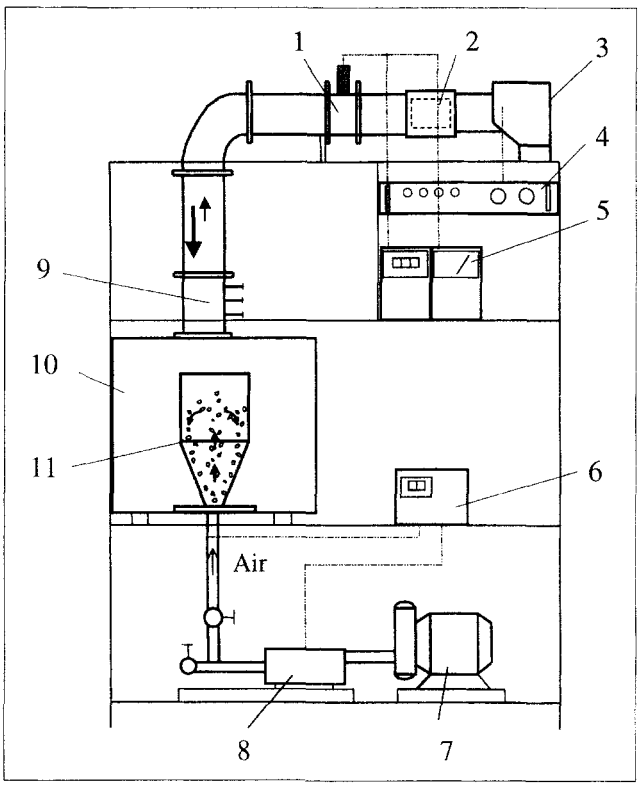

Figure 1. 2.45-GHz microwave and spouted-bed combined drying system.

(1) Direction coupler; (2) circulator; (3) magnetron; (4) power controller; (5) power meter; (6) temperature controller; (7) air pump; (8) heater; (9) three-stub tuner; (10) microwave cavity; (11) spouted bed.

2.1 m/s in all the tests. This velocity was able to provide stable particle circulation during drying to ensure uniform heating. Forty grams of diced apples were used in each drying test. Moisture loss was monitored by periodically weighing the sample on an electric balance (± 0.01 g). The average moisture content of samples was determined using the vacuum-oven method (AOAC, 1990). The drying temperature at the core of the dice was determined by measuring the inner temperature of ten randomly chosen apple pieces with a type-T thermocouple (response time 0.8 s) at predesignated time intervals. The pressure was measured using fresh apples with a fiber-optical pressure probe, which has a resolution of 1 kPa. The probe was passed through a hole opened on the wall of the spouted bed and carefully inserted into the center of a fresh-cut apple sample sealed with vacuum grease to prevent leakage of vapor. A data logging system was used to record the pressure data.

Model Validation

Predicted and experimentally determined moisture contents for MWSB and spouted-bed drying are compared in Figure 2 for diced apples. For MWSB drying, the means of four replicates were reported, and drying tests were conducted at microwave power density of 4 W/g (based on wet

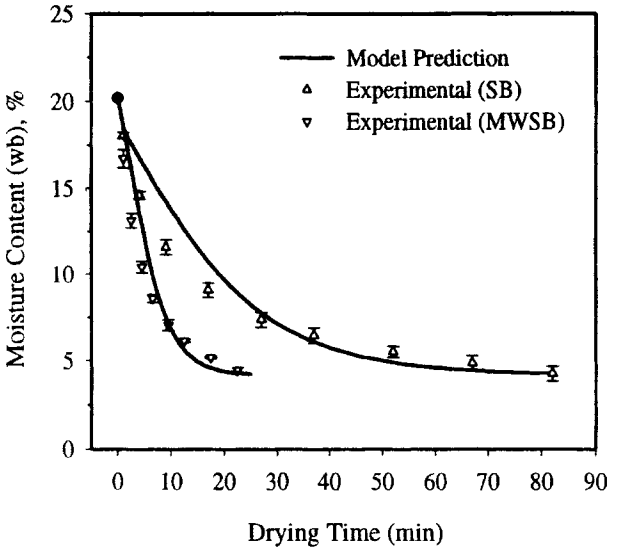

Figure 2. Moisture content: model prediction vs. experimental results for MWSB (microwave power = 4 Wg, air temperature = 70°C) and SB (air temperature = 70°C) drying.

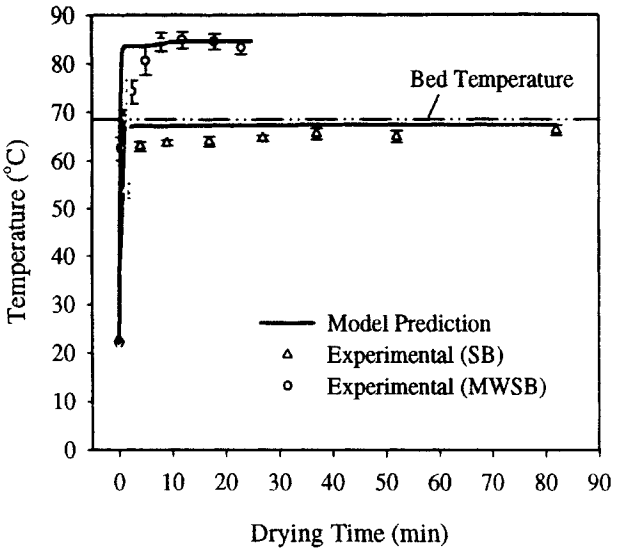

Figure 3. Temperature: model prediction vs. experimental results for MWSB (microwave power = 4 W/g, air temperature = 70°C) and SB (air temperature = 70°C), bed temperature = 68.5°C) drying.

material) and hot air temperature of 70°C. For spouted-bed drying, the same air conditions as MWSB drying were used, and experiments were triplicated. Repeatability is indicated by error bars in the figures. The simulated moisture content followed an exponential decay curve that characterizes the drying in the falling-rate period for hygroscopic materials (Figure 2). Generally, simulation predictions are in good agreement with experiments for both drying methods. Simulation slightly underestimated moisture loss at the beginning of drying. The assumption of a sphere for apple dice may be a major reason for this discrepancy. The influence of this assumption should be more in spouted bed drying because the drying is dominated by heat transfer from the surface to interior of a particle and moisture transfer from interior to surface. The surface-to-volume ratio for a small cube of apple is larger than that for a sphere. Therefore, more moisture loss occurred in experiments than in the simulation for spouted-bed drying. Another source for the discrepancies between predictions and experiments could be attributed to the terms dropped as a result of scale analysis. Nevertheless, the simulation followed the general trend of the experimental drying curves.

The center temperatures of diced apples from experiments and predictions are compared in Figure 3 for MWSB (MW power 4 W/g, and air temperature 70°C) and spouted-bed (air temperature 70°C) drying. In MWSB drying, predicted temperatures agree well with measurements. At the beginning of the drying, the hot air and the microwave energy heated the apple dice from outside and inside, respectively. This resulted in a rapid rise in product temperature. When the apple-dice surface temperature surpassed the air temperature, the air started to cool the apple dice. The center temperature continued to increase as a result of microwave heating until it reached about 83°C, when a balance was established between the energy supplied by the microwave and the heat loss due to surface convective cooling and evaporative heat loss. The product temperature remained at a nearly constant level throughout the rest of the drying. This is a unique characteristic associated with MWSB drying. In conventional MW-assisted fixed-bed hot-air drying, product temperature experiences a monotonic increase toward the end of drying (Lu et al., 1999). This is a result of insufficient surface cooling due to a decrease in evaporation when moisture content is relatively low but still able to couple microwave energy to generate heat. Lu et al. postulated that the surface-heat-transfer rate is the key to prevent the monotonic temperature elevation in microwave drying. The high surface heat transfer in the spouted bed helped to maintain a nearly constant drying temperature in MWSB drying. This temperature leveling effect prevents the product from overheating and charring. Therefore, MWSB drying can be especially useful for drying of heat-sensitive products. For MWSB drying, one can observe a slight overestimation of product temperature during the first 5 to 10 min of drying. This corresponds to an underestimated moisture content in the moisture curve (Figure 2). The higher residual moisture would result in a higher microwave heat generation and hence a higher temperature. In spouted-bed drying, sample temperature approached air temperature at a slightly lower rate compared to that of MWSB drying. Overall, predicted product temperature agreed well with bed temperature during drying, with measured temperatures being not more than 4°C lower than the predicted temperature.

Pressure readings from the fiber-optical probe are compared with model prediction in Figure 4. Experiments to verify computer simulation results for pressure predictions were conducted under different conditions than experiments for moisture and temperature verification. Fresh apple samples in cylindrical shape (8 mm in diameter and 15 mm in length)

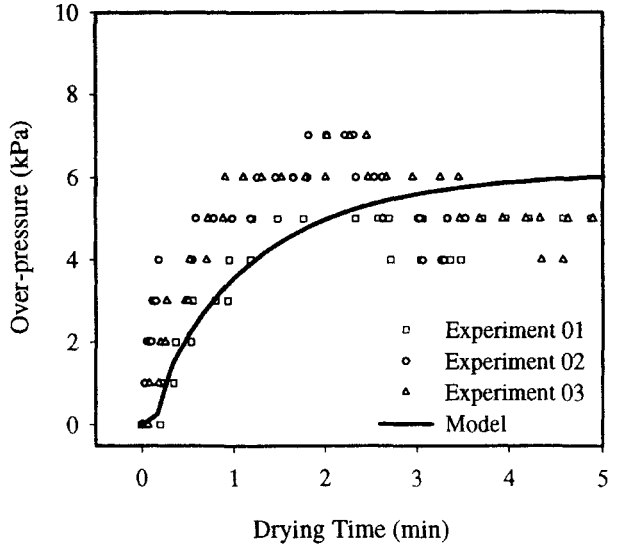

Figure 4. Pressure: MWSB drying with microwave power 10 W/g (based on wet material); hot-air temperature 70°C; and initial moisture content 84% (wet basis).

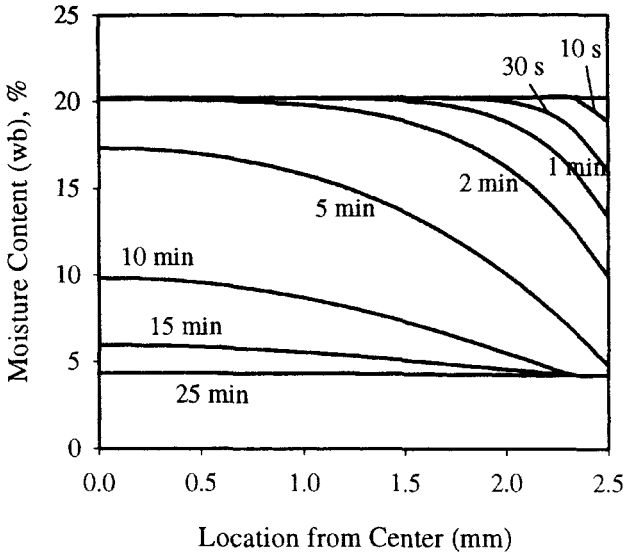

Figure 5. Moisture profile for MWSB drying with microwave power 4 W/g and hot-air temperature 70°C.

were used in the tests. The relatively large cylindrical sample permitted pressure measurement using a fiber-optical probe. In order to generate a vapor pressure above the threshold of the pressure probe (1 kPa), microwave power of 10 W/g and sample moisture of 84% (wb) were used. The measured pressure increased during the first 2 min of drying to reach a peak and started to decrease thereafter. At this stage, the moisture content of the sample remained high, and hence volumetric heating was still intensive and should be able to maintain the pressure. Therefore, the pressure decrease might have been caused by a gradual failure of the seal to the pressure probe. Model prediction underestimated pressure increase, probably due to the error in the empirical permeability equations used in the simulation. However, the model appears to yield results in good agreement with experiments.

It should to be mentioned that the model only applies to situations defined by the assumptions used in the study. To apply to other particulate materials, one must use appropriate thermophysical, transport, and dielectric properties for the materials. Microwave penetration depth in the material must be significantly larger than the particle diameter.

Results and Discussion

In commercial drying applications, apples are dried in two steps. First, fresh diced apples are dried to about 20–25% (wb) moisture content to produce so-called "evaporated apples." These apples are used for making pie filler and other products. Hot air drying for this stage is effective because of the relatively high final moisture content. Evaporated apples can be later dried in a second hot-air dryer to 3–5% (wb) moisture content to produce "dehydrated apples" for use in breakfast cereals or similar products. Hot-air drying at this stage is inefficient because the drying is in the falling-rate period. Feng and Tang (1998) demonstrated that MWSB drying was particularly effective in this stage to reduce drying time and maintain a relatively low drying temperature. Computer simulations were therefore used to study moisture migration and the effect of drying parameters for MWSB drying of apples from 20.2% to 5% moisture content (wb).

Figure 5 shows the predictive moisture profile for MWSB drying at a microwave power density of 4 W/g (wb) and hot-air temperature of 70°C. At the beginning of the drying, moisture migration took place only at the sample's surface. The center moisture remained unchanged for about 2 min of drying. In microwave heating/drying of high-moisture products, a surface moisture accumulation and even pumping has been reported (Constant et al., 1996; Ni et al., 1999). In Figure 5 we can see a large moisture gradient near the surface during the first 2 min. The rapid surface moisture removal due to this large moisture gradient at the product surface in diced apples (20.4%, wb) prevented surface moisture from accumulating.

It is interesting to examine the moisture fluxes in MWSB drying. Figure 6 shows the ratio of diffusive flux to moisture flux caused by pressure gradient at different drying times. The diffusive flux is given by

$$n_d = (1-\epsilon)\rho_s D_{\text{eff}} \frac{\partial X}{\partial r}, \tag{54}$$

while the pressure-driven flux is determined by

$$n_p = \frac{K k_{rf} \rho_f}{\mu_f} \frac{\partial P_g}{\partial r}. \tag{55}$$

The magnitude of diffusive flow is only half of the flow caused by total pressure gradient at the beginning of the drying along all nodes except the ones in the vicinity of the sample surface

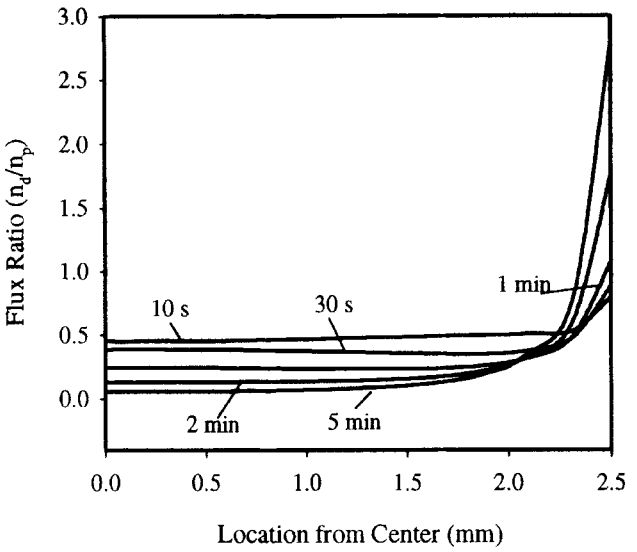

Figure 6. Ratio of diffusive flux to capillary flow flux as function of location for MWSB drying with microwave power 4 W/g and hot-air temperature 70°C.

(Figure 6). As the drying proceeds, moisture migration due to diffusion becomes less important, as indicated by the continuous decrease in the flux ratio. The high flux ratio found at the surface, however, must be related to a relatively high moisture gradient (Figure 5) and relative small pressure gradient (see Figure 9) near the surface. The flux ratio presented in Figure 6 reveals that in MWSB drying, the pressure-gradient-driven flow plays an important role in moisture migration. A comparison of drying rate between spouted-bed drying and MWSB drying is presented in Figure 7. The drying rate in diced apples during spouted-bed drying is a fraction of that of the MWSB drying when moisture content is relatively high. When moisture is low, the drying-rate ratio decreases even further. The only difference between spouted-bed and MWSB drying is the addition of microwave energy. The internal heat generation due to microwave heating results in internal pressure build-up, which facilitates the pressure-driven moisture migration. Combining these findings in Figures 6 and 7, one can see that (1) the pressure-driven flow of moisture results in a high drying rate in MWSB drying, and (2) microwave drying is more effective when moisture content is low where the moisture transport due to gradient in moisture content becomes insignificant.

The temperature profiles in the diced apples for MWSB drying with 4 W/g microwave power and 70°C air temperature are shown in Figure 8. In the first minute, the temperature of diced apple increases rapidly due to heating by both hot air and microwave energy. The temperature profile in diced apples during this period was relatively flat. When the surface temperature surpassed the air temperature (70°C) after about 30 s of drying, a positive temperature gradient was established. When compared with Figure 5, it is seen that the temperature gradient is in the same direction as the moisture gradient, hence helping to enhance the drying.

The pressure development during MWSB drying is shown in Figure 9. Pressure increased until it reached a maximum after about 5 min of drying. About 50% of the initial moisture was removed during this period (Fig. 2). The ability of the residual moisture to generate vapor pressure decreased in relation to the sorption relation. A reduction in pressure is now observed. The pressure gradient reached its maximum near the surface during the first minute of drying. This is partially responsible for the rapid loss of surface moisture, as presented in Figure 5. After 5 min, however, an overall pressure gradient along the radius of the apple dice was established, helping to transport moisture from inside to the surface. After 15 min, the internal pressure approached the external pressure.

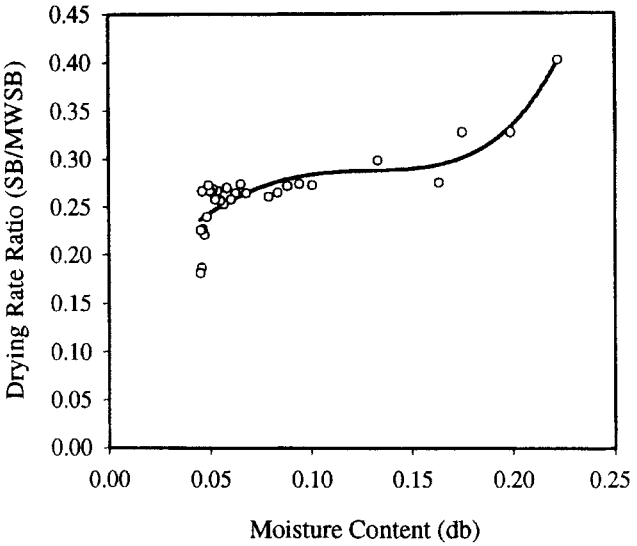

Figure 7. Ratio of SB drying rate to MWSB drying rate for MWSB drying at microwave power 4 W/g and hot-air temperature 70°C and SB drying at 70°C.

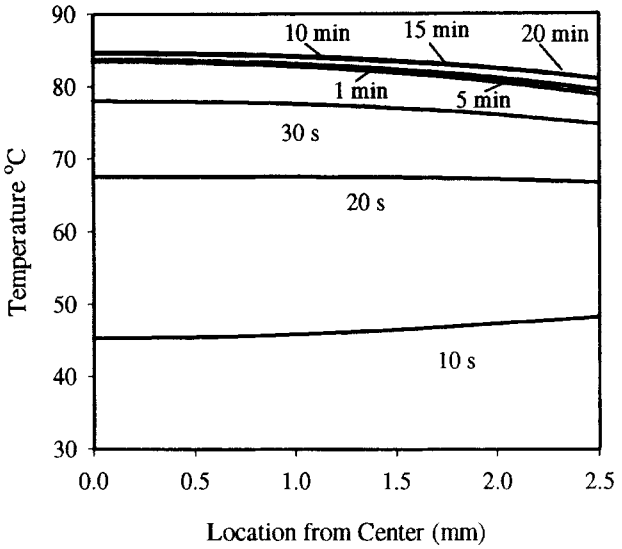

Figure 8. Temperature profile for MWSB drying with microwave power 4 W/g and hot-air temperature 70°C.

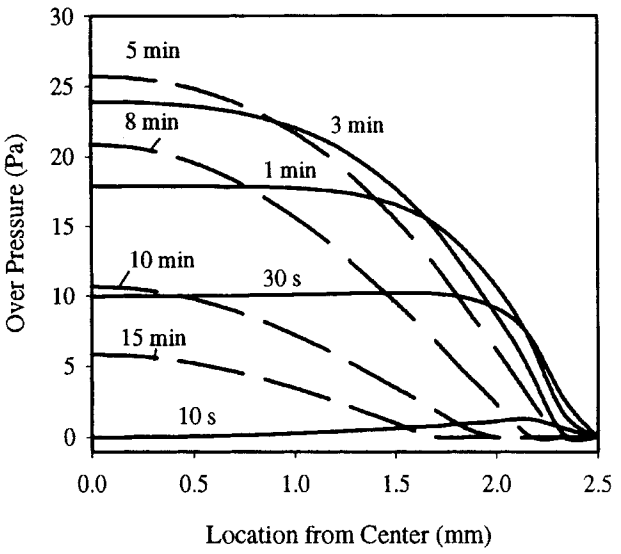

Figure 9. Pressure profile for MWSB drying with microwave power 4 W/g and hot-air temperature 70°C.

The internal vapor pressure increased with microwave power. This is shown in Figure 10. During MWSB drying of diced apples with an initial moisture of 20.2% (wb), maximum vapor pressure was generated within the first 5 min of drying. Higher microwave power resulted in a higher pressure due to more internal heat generation. As power decreased, the maximum vapor pressure decreased and the time corresponding to the maximum pressure increased. The higher pressure resulted in a more rapid moisture reduction, which, in turn, reduced the product's ability to sustain the peak vapor pressure. When power was reduced to 0 W/g, a less noticeable pressure build-up was observed. This suggests that moisture migration due to the vapor-pressure gradient in hot-air drying was significantly lower than with MWSB drying.

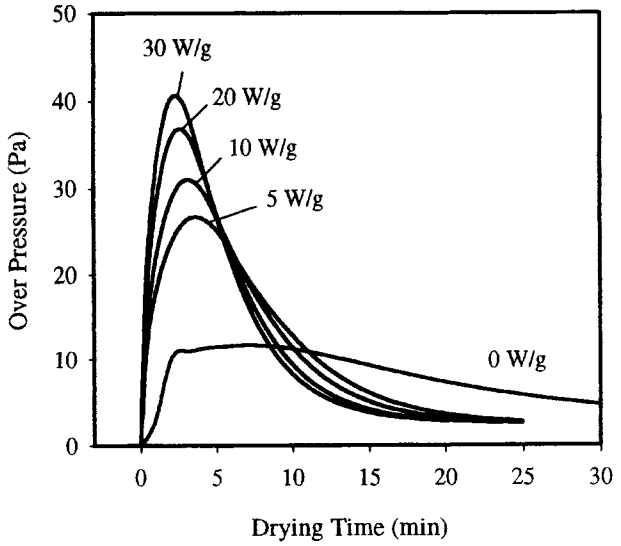

Figure 10. Over pressure for MWSB drying at different microwave power levels.

Conclusions

The heat- and mass-transfer model developed in this study can be used as an effective tool to predict moisture, temperature, and pressure history and distribution for microwave and spouted-bed drying (MWSB) of particulate materials. The model's prediction of moisture, temperature, and pressure agree with experimental results. A temperature-leveling effect was predicted and is in agreement with experimental results. This unique temperature-leveling feature in MWSB drying makes it possible for use on heat-sensitive products in drying. The internal pressure build-up in MWSB drying resulted in a dominant pressure-driven flow in diced apples. Microwave heating is more effective when moisture content is low.

Acknowledgments

This project was supported by Washington State University IMPACT Center and Northwest Center for Small Fruits Research. The authors thank Timothy Wig and Wayne DeWitt for assistance in developing the 2.45-GHz MWSB drying system, and TreeTop, Inc., Selah, WA, for donating evaporated apples.

Notation

C = capacity coefficient
C_p = specific heat, $J \cdot kg^{-1} \cdot K^{-1}$
d_p = particle diameter, m
D = kinetic coefficient; material derivative
D_{av} = binary air–vapor diffusivity, $m^2 \cdot s^{-1}$
D_b = bound water diffusivity, $m^2 \cdot s^{-1}$
D_c = diameter of the spouted-bed column, m
F = heat or mass flux at boundaries, $J \cdot m^{-2} \cdot s^{-1}$ or $kg \cdot m^{-2} \cdot s^{-1}$
g = gravitational acceleration, $m \cdot s^{-2}$
h = enthalpy, $J \cdot kg^{-1}$; surface-heat-transfer coefficient, $W \cdot m^{-2} \cdot K^{-1}$
h_m = mass-transfer coefficient, $m \cdot s^{-1}$
Δh_v = latent heat of free water, $J \cdot kg^{-1}$
H = sample thickness, m
H_0 = initial bed height, m
j = diffusive mass flux, $kg \cdot m^{-2} \cdot s^{-1}$
k_r = relative permeability
m = mass, kg
$\dot{m}$ = moisture evaporation rate, $kg \cdot m^{-3} \cdot s^{-1}$
M = molar mass, $kg \cdot mol^{-1}$
$\dot{M}$ = total moisture evaporation rate, $kg \cdot m^{-3} \cdot s^{-1}$
n = mass flux, $kg \cdot m^{-2}\ s^{-1}$; a vector normal to the surface (outwardly)
N = total node number
P = pressure, Pa; microwave power, W
P_c = capillary pressure, Pa
q = heat flux, $J \cdot m^{-2} \cdot s^{-1}$
R = sample radius, m^{-1}
R' = universal gas constant, $J \cdot mol^{-1} \cdot K^{-1}$
S = saturation
t = time, s
T = average absolute temperature, K
TL = iteration limit for time, s^{-1}
u = superficial average velocity, $m \cdot s^{-1}$
U = spouted-bed air superficial velocity, $m \cdot s^{-1}$
X = moisture content (dry basis), kg H_2O · (kg solid)$^{-1}$

X' = moisture content (wet basis), kg H_2O·(kg wet material)$^{-1}$
W = mass, kg

Greek letters

δ = finite difference element thickness, m
ϵ = porosity [(gas + liquid)/total volume], tolerance limit on iteration scheme
ϵ' = porosity defined in Eq. 38 (gas volume/total volume); dielectric constant,
ϵ'' = loss factor
γ = angle of conical base in the spouted bed, degree
ϕ = shape factor = 1/sphericity
Φ = heat source, W·m^{-3}
λ = thermal conductivity, W·m^{-1}·K^{-1}; wave length, m
μ = dynamic viscosity, kg·m^{-1}·s^{-1}
ρ = density, kg·m^{-3}
ρ_s = solid density (solid mass/solid volume), kg·m^{-3}
$\bar{\tau}$ = shear-stress tensor, kg·m^{-2}
ζ = parameter defined in Eq. 40

Subscripts and superscripts

0 = at saturated condition or free space; initial condition (refers to fresh sample)
a = air
atm = atmospheric pressure
b = bound water, bulk density
c = velocity or temperature scales
eff = effective
f = free water
g = gas = air + vapor
i = space step in finite difference scheme
l = liquid = free water + bound water
max = maximum values
p = particle
P = pressure
s = solid, or relating to surface
T = temperature
v = vapor
w = total moisture = free water + bound water + vapor
X = moisture
∞ = surrounding

Dimensionless groups

$$\text{Particle Archimedes number} = Ar = \frac{g d_p^3 \rho_{a\infty}(\rho_{pb} - \rho_{a\infty})}{\mu_{a\infty}^2}$$

$$\text{Particle Reynolds number} = \text{Re} = \frac{U d_p \rho_{a\infty}}{\mu_{a\infty}}$$

Literature Cited

Adu, B., and L. Otten, "Modeling Microwave Heating Characteristics of Granular Hygroscopic Solids," *J. Microwave Power Electromagn. Energy*, **31**, 35 (1996).

AOAC, *Official Methods of Analysis*, 15th ed., Assoc. of Official Analytical Chemists (1990).

Bird, R. B., W. E. Stewart, and E. N. Lightfoot, *Transport Phenomena*, Wiley, New York (1960).

Bories, S. A., "Fundamentals of Drying of Capillary-Porous Bodies," *Convective Heat and Mass Transfer in Porous Media*, S. Kakac, B. Kilkis, F. A. Kulacki, and F. Arinc, eds., Kluwer Academic, Dordrecht, The Netherlands (1991).

Chen, P., and D. C. T. Pei, "A Mathematical Model of Drying Processes," *Int. J. Heat Mass Transfer*, **32**, 297 (1989).

Chen, P., and P. S. Schmidt, "An Integral Model for Drying of Hygroscopic and Nonhygroscopic Materials with Dielectric Heating," *Drying Technol.*, **8**, 907 (1990).

Constant, T., C. Moyne, and P. Perré, "Drying with Internal Heat Generation: Theoretical Aspects and Application to Microwave Heating," *AIChE J.*, **42**, 359 (1996).

Donsì, G., G. Ferrari, and R. Nigro, "Experimental Determination of Thermal Conductivity of Apple and Potato at Different Moisture Contents," *J. Food Eng.*, **30**, 263 (1996).

Feng, H., and J. Tang, "Microwave Finish Drying of Diced Apples in a Spouted Bed," *J. Food Sci.*, **63**, 679 (1998).

Feng, H., J. Tang, and R. Cavalieri, "Combined Microwave and Spouted Bed Drying of Diced Apples: Effect of Drying Conditions on Drying Kinetics and Product Temperature," *Drying Technol.*, **17**, 1981 (1999).

Feng, H., *Microwave Drying of Particulate Foods in a Spouted Bed*, PhD Diss., Washington State Univ., Pullman (2000).

Feng, H., J. Tang, and G. Plumb, "Intrinsic and Relative Permeability for Flow of Humid Air in Unsaturated Apple Tissues," *J. Food Eng.* (2001a).

Feng, H., J. Tang, and R. Cavalieri, "Dielectric Properties of Dehydrated Apples as Affected by Moisture and Temperature," *Trans. ASAE* (2001b).

Garcia, R., F. Leal, and C. Rolz, "Drying of Bananas Using Microwave and Air Ovens," *Int. J. Food Sci. & Technol.*, **23**, 81 (1988).

Goedeken, D. L., and C. H. Tong, "Permeability Measurements of Porous Food Materials," *J. Food Sci.*, **58**, 1329 (1993).

Gong, L., *A Theoretical, Numerical and Experimental Study of Heat and Mass Transfer in Wood During Drying*, PhD Diss., Washington State University, Pullman (1992).

Jansen, W., and B. van der Wekken, "Modeling of Dielectrically Assisted Drying," *J. Microwave Power Electromagn. Energy*, **26**, 227 (1991).

Jolly, P., and I. Turner, "Microwave Drying of Porous Media," *Proc. Australasian Heat and Mass Transfer Conf.*, Univ. of Canterbury, Christchurch, New Zealand, p. 331 (1989).

Krokida, M. K., and Z. B. Maroulis, "Effect of Microwave Drying on Some Quality Properties of Dehydrated Products," *Drying Technol.*, **17**, 449 (1999).

Le Pourhiet, A., S. Bories, and D. Bialod, "Drying Simulation of Hygroscopic Media—Applications with Use of Microwaves," *Proc. Int. Drying Symp.*, J. C. Ashworth, ed., England, p. 429 (1982).

Lian, G., C. S., R. E. Harris, and M. Warboys, "Coupled Heat and Moisture Transfer During Microwave Vacuum Drying," *J. Microwave Power Electromagn. Energy*, **32**, 34 (1997).

Lu, L., J. Tang, and X. Ran, "Temperature and Moisture Changes During Microwave Drying of Sliced Food," *Drying Technol.*, **17**, 413 (1999).

Markowski, A. S., "Drying Characteristics in a Jet-Spouted Bed Dryer," *The Can. J. Chem. Eng.*, **70**, 938 (1992).

Mohsenin, N. N., *Physical Properties of Plant and Animal Materials*, Gordon & Breach, Amsterdam (1986).

Moyne, C., and P. Perre, "Processes Relation to Drying: I. Theoretical Model," *Drying Technol.*, **9**, 1135 (1991).

Mullin, J., "Microwave Processing," *New Methods of Food Preservation*, G. W. Gould, ed., Blackie, London, p. 112 (1995).

Ni, H., A. K. Datta, and K. W. Torrance, "Moisture Transport in Intensive Microwave Heating of Biomaterials: A Multiphase Porous Media Model," *Int. J. Heat Mass Transfer*, **42**, 1501 (1999).

Niesteruk, R., "Changes of Thermal Properties of Fruits and Vegetables During Drying," *Drying Technol.*, **14**, 415 (1996).

Plumb, O. A., L. M. Couey, and D. Shearer, "Contact Drying of Wood Veneer," *Drying Technol.*, **4**, 387 (1986).

Prabhanjan, D. G., H. S. Ramaswamy, and G. S. V. Raghavan, "Microwave-Assisted Convective Air Drying of Thin Layer Carrots," *J. Food Eng.*, **25**, 283 (1995).

Roman, G. N., M. J. Urbicain, and E. Rotstein, "Moisture Equilibrium in Apples at Several Temperatures: Experimental Data and Theoretical Considerations," *J. Food Sci.*, **47**, 1484 (1982).

Stanish, M. A., G. S. Schajer, and F. Kayihan, "A Mathematical Model of Drying for Hygroscopic Porous Media," *AIChE J.*, **32**, 1301 (1986).

Torringa, E. M., E. J. van Dijk, and P. S. Bartels, "Microwave Puffing of Vegetables: Modeling and Measurements," *Proc. Microwave Power Symp.*, Int. Microwave Power Inst. (1996).

Turner, I. W., and P. G. Jolly, "Combined Microwave and Conventional Drying of a Porous Material," *Drying Technol.*, **9**, 1209 (1991).

Turner, I. W., *The Modeling of Combined Microwave and Convective*

Drying of a Wet Porous Material, PhD Thesis, Univ. of Queensland, Brisbane, Qld., Australia (1991).
Turner, I. W., J. R. Puiggali, and W. Jomaa, "A Numerical Investigation of Combined Microwave and Convective Drying of a Hygroscopic Porous Material: A Study Based on Pine Wood," *Trans. Inst. Chem. Eng.*, **76**, (Pt. A), 193 (1998).
Wei, C. K., H. T. Davis, E. A. Davis, and J. Gorden, "Heat and Mass Transfer in Water-Laden Sandstone: Microwave Heating," *AIChE J.*, **31**, 842 (1985).
Whitaker, S., "Simultaneous Heat, Mass, Momentum Transfer in Porous Media: A Theory of Drying," *Advances in Heat Transfer*, Vol. 13, Academic, New York, p. 119 (1977).
Willian Deen, M., *Analysis of Transport Phenomena*, Oxford Univ. Press, New York (1998).

Appendix

Coefficients in microwave drying governing equations are given in the following list:

$$D_X^f = -\frac{1}{1-\epsilon}\frac{\rho_f}{\rho_s}\frac{Kk_{rf}}{\mu_f}\left(\frac{\partial P_c}{\partial X_w}\right)_T$$

$$D_T^f = -\frac{1}{1-\epsilon}\frac{\rho_f}{\rho_s}\frac{Kk_{rf}}{\mu_f}\left(\frac{\partial P_c}{\partial T}\right)_{X_w} \tag{A1}$$

$$D_P^f = \frac{1}{1-\epsilon}\frac{\rho_f}{\rho_s}\frac{Kk_{rf}}{\mu_f}$$

$$D_X^b = \frac{1-\epsilon'}{1-\epsilon}\frac{D_b}{\rho_s}\frac{\epsilon R'T}{P_v M_v}\left(\frac{\partial P_v}{\partial X_w}\right)_T$$

$$D_T^b = -\frac{1-\epsilon'}{1-\epsilon}\frac{D_b}{\rho_s}\left[\frac{S_v}{M_v} - \frac{\epsilon R'T}{P_v M_v}\left(\frac{\partial P_v}{\partial T}\right)_{X_w}\right] \tag{A2}$$

$$D_P^b = 0$$

$$D_X^v = \frac{D_{av}P_g}{(1-\epsilon)\rho_s}\frac{M_a M_v}{R'T\left(P_g M_a + (M_v - M_a)P_v\right)}\left(\frac{\partial P_v}{\partial X_w}\right)_T$$

$$D_T^v = \frac{D_{av}P_g}{(1-\epsilon)\rho_s}\frac{M_a M_v}{R'T\left(P_g M_a + (M_v - M_a)P_v\right)}\left(\frac{\partial P_v}{\partial T}\right)_{X_w} \tag{A3}$$

$$D_P^v = \frac{1}{(1-\epsilon)\rho_s}\left[\frac{P_v M_v}{R'T}\frac{Kk_{rg}}{\mu_g} - \frac{D_{av}M_a M_v P_v}{R'T\left(P_g M_a + (M_v - M_a)P_v\right)}\right].$$

Equations A1 to A3 are coefficients that correspond to the moisture transport in the forms of free water (f), bound water (b), and vapor (v) driven by moisture (X), temperature (T), and pressure gradient (P):

$$C_{TX} = \Delta h_v \frac{M_v}{R}\left\{-\frac{(1-\epsilon)\rho_s}{\rho_f+\rho_b}\frac{P_v}{T} + \left[\epsilon - \frac{(1-\epsilon)\rho_s}{\rho_f+\rho_b}X_l\right]\frac{1}{T}\frac{\partial P_v}{\partial X_l}\right\} \tag{A4}$$

$$C_{TT} = (\rho C_p)_{\text{eff}} + \Delta h_v \frac{M_v}{R'}\left[\epsilon - \frac{(1-\epsilon)\rho_s}{\rho_f+\rho_b}X_l\right]\frac{\partial(P_v/T)}{\partial T} \tag{A5}$$

$$D_{TX} = \Delta h_v(1-\epsilon)\rho_s D_X^v$$
$$D_{TT} = \lambda_{\text{eff}} + \Delta h_v(1-\epsilon)\rho_s D_T^v \tag{A6}$$
$$D_{TP} = \Delta h_v(1-\epsilon)\rho_s D_P^v.$$

Equations A4–A6 are coefficients in Eq. 21:

$$C_{PX} = \frac{\epsilon M_a}{R'}\left[-\frac{P_g - P_v}{T}\left(\frac{1-\epsilon}{\epsilon}\frac{\rho_s}{\rho_f+\rho_b}\right) - \left(1 - \frac{1-\epsilon}{\epsilon}\frac{\rho_s}{\rho_f+\rho_b}X_l\right)\frac{1}{T}\frac{\partial P_v}{\partial X_l}\right]$$

$$C_{PT} = \frac{\epsilon M_a}{R'}\left(1 - \frac{1-\epsilon}{\epsilon}\frac{\rho_s}{\rho_f+\rho_b}X_l\right)\left(\frac{P_g}{T^2} - \frac{\partial(P_v/T)}{\partial T}\right) \tag{A7}$$

$$C_{PP} = \frac{\epsilon M_a}{R'}\left(1 - \frac{1-\epsilon}{\epsilon}\frac{\rho_s}{\rho_f+\rho_b}X_l\right)\frac{1}{T}$$

$$D_X^a = -(1-\epsilon)\rho_s D_X^v = -D_{av}\frac{M_v}{R'T}\frac{P_g M_a}{P_g M_a + (M_v - M_a)P_v}\left(\frac{\partial P_v}{\partial X_w}\right)_T$$

$$D_T^a = -(1-\epsilon)\rho_s D_T^v = -D_{av}\frac{M_v}{R'T}\frac{P_g M_a}{P_g M_a + (M_v - M_a)P_v}\left(\frac{\partial P_v}{\partial T}\right)_{X_w} \tag{A8}$$

$$D_P^a = \frac{(P_g - P_v)M_a}{R'T}\frac{Kk_{rg}}{\mu_g} + D_{av}\frac{M_v}{R'T}\frac{P_v M_a}{P_g M_a + (M_v - M_a)P_v}.$$

Equations A7 and A8 are coefficients in the pressure equation (Eq. 22):

$$D'_X = X_0 D_X; \qquad D'_T = (T_{\max} - T_0)D_T;$$
$$D'_P = (P_{\max} - P_{\text{atm}})D_P \qquad D'_{TX} = X_0 D_{TX};$$
$$D'_{TT} = (T_{\max} - T_0)D_{TT}; \qquad D'_{TP} = (P_{\max} - P_{\text{atm}})D_{TP};$$
$$D'^a_X = X_0 D^a_x; \qquad D'^a_T = (T_{\max} - T_0)D^a_T;$$
$$D'^a_p = (P_{\max} - P_{\text{atm}})D^a_P. \tag{A9}$$

Equations A9 gives the coefficients in the simplified drying equations (Eqs. 31–33).

$$\zeta = 1 - \frac{1-\epsilon}{\epsilon}\frac{\rho_s}{\rho_f+\rho_b}X_l. \tag{A10}$$

Equation A10 is a coefficient in Eq. 40.

Manuscript received Aug. 14, 2000, and revision received Jan. 16, 2001.